Polaritons in semiconductor multilayered materials

Alain Dereux, Jean-Pol Vigneron, Philippe Lambin, and Amand A. Lucas
Institute for Studies in Interface Sciences, Facultés Universitaires Notre-Dame de la Paix, 61 rue de Bruxelles, B-5000 Namur, Belgium
(Received 7 December 1987)

A distinctive feature of multilayered semiconductor structures lies in the fact that their reflectance and absorption spectra are strongly influenced by their stratified geometry. With use of a standard Green's-function technique, the concept of a local density of polariton modes is examined and its formulation in terms of planar impedances is carried out. This scattering-theoretic approach appears to be valid for materials with any graded dielectric response and allows detailed description of the spatial distribution of the electromagnetic energy in nonradiative or radiative polariton modes at a given frequency and wavelength. In a multilayered material, the influence of the interfacial structure of the sample on the spectral properties such as the reflectance and attenuated total reflection is depicted. Various semiconductor layered structures are considered and their spectral properties in both polarizations, transverse electric and transverse magnetic, are analyzed in terms of local density of polariton modes. This paper basically describes complex states built from interacting interfaces or confined states and accounts for their localization. In the transverse-magnetic polarization, the spatial distribution of modes demonstrates that multilayered structures are able to absorb electromagnetic energy by a process involving interfacial polaritons. Finally, the long-wavelength limit of our formalism will be developed further to explicitly show its connection with the well-known effective-medium theory and to discuss the importance of the form anisotropy of the superlattice structure.

I. INTRODUCTION

Semiconducting multilayered structures, including synthesized semiconductor superlattices are basic to the development of many new electronic and optical devices.[1] Considerable efforts are devoted to the improvement of growth techniques and sample quality of these heterogeneous structures, while concurrently their physical properties, mainly electronic and vibrational, are actively investigated.[2] Recent works[3–9] report experimental and theoretical results on the application of several spectroscopies to such multilayer structures, demonstrating some of the consequences of the accumulation of interfaces on their response to electromagnetic probes.

This paper considers these multilayered materials from the point of view of their long-wavelength dielectric response. It emphasizes the relationship between the electromagnetic excitations and the results of several types of spectroscopies which deal with the retarded dielectric response of the synthetic material. The application of infrared reflectance spectroscopy in transverse-electric (TE) or transverse-magnetic (TM) polarizations, and the measurement of attenuated total internal reflection spectra are considered as possible probes of the influence of the stratification on collective excitations, such as long-wavelength phonons or plasmons in multilayered systems.

The theory reported in this paper is that of polariton modes of a general stratified medium. We first reexamine the electrodynamics of a crystalline material presenting a spatial variation of its dielectric function in the direction of growth (Fig. 1) to describe in detail the radiative and nonradiative states generated in this geometry. The definition of an electromagnetic Green's function based on the concept of planar impedance allows one to study the continuous parts of the spectrum, complementing earlier descriptions of the discrete electromagnetic surface modes. In particular, the local density of polariton states introduced in this paper proves to be a powerful tool for investigating the effect of stratification on various material response functions, by illustrating the spatial distribution of collective modes along the growth axis. Moreover, this quantity can directly be related to the spectral properties of heterostructures as it takes account not only of the normal modes but also of the virtual or resonant modes influenced by finite lifetime effects.

Since the planar impedance emerges as the basic ingredient for a combined study of the polariton structure and the various related spectroscopies, we next show that this quantity can be obtained in a simple way for complex multilayered system, avoiding the cumbersome algebra implied by the usual transfer matrix approach. In our treatment, the dielectric function needs not take the shape of an histogram: it is equally applicable to any graded dielectric medium, provided that the definition of a local dielectric function remains acceptable on the scale of the system inhomogeneities.

Infrared optical properties of structures made of thin layers of polar materials directly depend on the polariton structure, in the radiative regime, and, to some extent, the nonradiative regime as well. In this paper, simulated spectra are interpreted in terms of local densities of polariton modes and provide illustrations of vibrational properties for multilayered semiconductors whose complexity ranges from a simple homogeneous crystal to a semi-infinite superlattice.

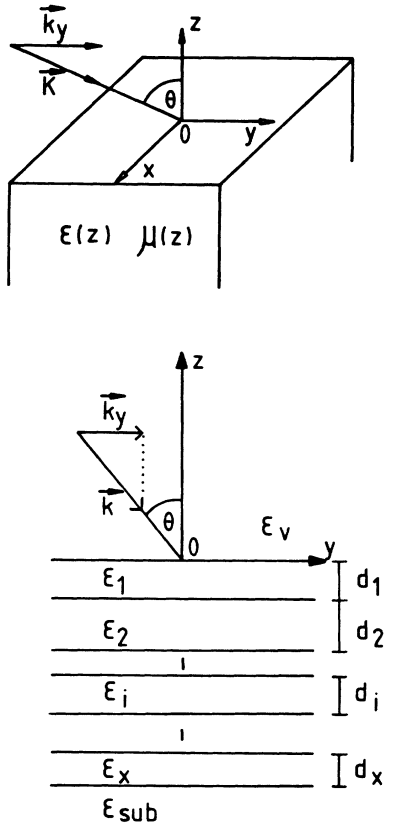

FIG. 1. Geometry of interest for (a) general stratified media and (b) multilayered structures.

II. POLARITON MODES

The stratified dielectric material considered in this paper consists of a semi-infinite medium characterized by a long-wavelength dielectric, isotropic constant $\epsilon(z)$, and a magnetic permittivity $\mu(z)$ which vary only in a direction perpendicular to its surface (Fig. 1), that is the direction of the material growth. Due to the stratification, the application of an electric field to such a material results in a macroscopic polarization involving induced charges associated with the dielectric function gradients. The polariton modes can easily be predicted from classical electrodynamics. In fact, most of the physics of the electromagnetic wave propagation in a stratified medium is already known from previous works in optics.[10–13] It has long been shown that the electric and the magnetic fields (**E** and **H**) can both be extracted from the solution of a one-dimensional equation, different for transverse-electric modes (TE, or *s*-polarized) and transverse-magnetic modes (TM, or *p*-polarized): for electric and magnetic fields oscillating at the angular frequency ω and for the geometry described in Fig. 1, Maxwell's equations lead to simple solutions, invariant under a translation in the x direction. For a TM mode ($E_x=0, H_y=H_z=0$), the fields are explicitly given by

$$H_x = e^{ik_y y} W_p(z) , \tag{2.1a}$$

$$E_y = \frac{-1}{i\omega\epsilon_0\epsilon(z)} \frac{\partial H_x}{\partial z} , \tag{2.1b}$$

$$E_z = \frac{1}{i\omega\epsilon_0\epsilon(z)} \frac{\partial H_x}{\partial y} , \tag{2.1c}$$

where $W_p(z)$ satisfies the one-dimensional wave equation

$$\epsilon(z)\frac{d}{dz}\left[\frac{1}{\epsilon(z)}\frac{dW_p(z)}{dz}\right] - k^2(z)W_p(z) = 0 . \tag{2.2}$$

For a TE mode (*s*-polarized: $H_x=0, E_y=E_z=0$), one finds in the same way

$$E_x = e^{ik_y y} W_s(z) , \tag{2.3a}$$

$$H_y = \frac{1}{i\omega\mu_0\mu(z)} \frac{\partial E_x}{\partial z} , \tag{2.3b}$$

$$H_z = \frac{-1}{i\omega\mu_0\mu(z)} \frac{\partial E_x}{\partial y} \tag{2.3c}$$

with

$$\mu(z)\frac{d}{dz}\left[\frac{1}{\mu(z)}\frac{dW_s(z)}{dz}\right] - k^2(z)W_s(z) = 0 . \tag{2.4}$$

In these equations, $k^2(z)=k_y^2-(\omega/c)^2\epsilon(z)\mu(z)$ where k_y is the radiation wave vector parallel to the sample surface, and c denotes the velocity of light in vacuum. The functions $W_p(z)$ and $W_s(z)$ are continuous functions of z, even if $\epsilon(z)$ or $\mu(z)$ experience finite discontinuities. This is also true for $[1/\mu(z)][dW_s(z)/dz]$ and $[1/\epsilon(z)][dW_p(z)/dz]$, as can be seen from the usual electromagnetic field matching conditions.

Since $W_p(z)$ or $W_s(z)$ describe the electromagnetic fields propagating inside the crystal, they characterize the coupling between polarization waves in the crystal and the external electromagnetic probe. In the energy range considered in this paper, these coupled modes are phonon polaritons arising from the coupling of lattice vibrations and the electromagnetic radiation. The various spectroscopies we shall deal with later can be interpreted in terms of polariton excitations, and more precisely, are connected to the local polariton density of states. The local density of states of polaritons at any depth along the z axis of the multilayered crystal is deduced from the Green's functions $G_p(z,z';k_y^2)$ and $G_s(z,z';k_y^2)$ associated with the wave equations governing the spatial variations $W_p(z)$ and $W_s(z)$. These Green's functions satisfy

$$\frac{\partial}{\partial z}\left[\frac{1}{\epsilon(z)}\frac{\partial G_p(z,z';k_y^2)}{\partial z}\right]+\left[\frac{-k_y^2}{\epsilon(z)}+\frac{\omega^2}{c^2}\mu(z)\right]G_p(z,z';k_y^2)=\delta(z-z') \quad (2.5)$$

and

$$\frac{\partial}{\partial z}\left[\frac{1}{\mu(z)}\frac{\partial G_s(z,z';k_y^2)}{\partial z}\right]+\left[\frac{-k_y^2}{\mu(z)}+\frac{\omega^2}{c^2}\epsilon(z)\right]G_s(z,z';k_y^2)=\delta(z-z') . \quad (2.6)$$

Both solutions $G_p(z,z';k_y^2)$ and $G_s(z,z';k_y^2)$ are continuous functions of z, even when $z=z'$. $\epsilon(z)^{-1}\partial G_p(z,z';k_y^2)/\partial z$ and $\mu(z)^{-1}\partial G_s(z,z';k_y^2)/\partial z$ are also continuous functions of z, except at $z=z'$. However, the following matching conditions hold:

$$\lim_{L\to 0}\left[\frac{1}{\epsilon(z'+L)}\frac{\partial G_p(z'+L,z';k_y^2)}{\partial z}-\frac{1}{\epsilon(z'-L)}\frac{\partial G_p(z'-L,z';k_y^2)}{\partial z}\right]=1 , \quad (2.7)$$

$$\lim_{L\to 0}\left[\frac{1}{\mu(z'+L)}\frac{\partial G_s(z'+L,z';k_y^2)}{\partial z}-\frac{1}{\mu(z'-L)}\frac{\partial G_s(z'-L,z';k_y^2)}{\partial z}\right]=1 . \quad (2.8)$$

In this one-dimensional problem, the Green's function $G_p(z,z';k_y^2)$ and $G_s(z,z';k_y^2)$ can be formulated as follows:

$$G_p(z,z';k_y^2)=\frac{W_{1p}(z_<)W_{2p}(z_>)}{W_{1p}(z')/\epsilon(z')[dW_{2p}(z)/dz]_{z=z'}-W_{2p}(z')/\epsilon(z')[dW_{1p}(z)/dz]_{z=z'}} , \quad (2.9)$$

$$G_s(z,z';k_y^2)=\frac{W_{1s}(z_<)W_{2s}(z_>)}{W_{1s}(z')/\mu(z')[dW_{2s}(z)/dz]_{z=z'}-W_{2s}(z')/\mu(z')[dW_{1s}(z)/dz]_{z=z'}} , \quad (2.10)$$

where $z_<$ is, as usual, the infimum of z and z' and $z_>$ their supremum. In these equations, $W_{1p}(z)$ and $W_{2p}(z)$ are the regular solutions of Eq. (2.2) which vanish, respectively, when z approaches $-\infty$ or $+\infty$ as k_y^2 assumes a (vanishingly small) positive imaginary part. $W_{1s}(z)$ and $W_{2s}(z)$ are similarly defined as regular solutions of Eq. (2.4).

Following standard results of the Green's-function theory, the local densities of modes are defined by

$$\rho_p(z;k_y^2)=-\mathrm{Im}[G_p(z,z;k_y^2)]/\pi \quad (2.11)$$

and

$$\rho_s(z;k_y^2)=-\mathrm{Im}[G_s(z,z;k_y^2)]/\pi . \quad (2.12)$$

The diagonal elements obtained from the above Green's-functions expressions are

$$G_p(z,z;k_y^2)=\frac{c/\omega}{\zeta_{p,+}(z)-\zeta_{p,-}(z)} \quad (2.13)$$

and

$$G_s(z,z;k_y^2)=\frac{c/\omega}{\zeta_{s,+}^{-1}(z)-\zeta_{s,-}^{-1}(z)} , \quad (2.14)$$

where we have defined

$$\zeta_{p,+}(z)=\lim_{L\to 0}\frac{c/\omega}{\epsilon(z+L)}\left[\frac{dW_{2p}(z)/dz}{W_{2p}(z)}\right]_{Z=Z+L} , \quad (2.15)$$

$$\zeta_{p,-}(z)=\lim_{L\to 0}\frac{c/\omega}{\epsilon(z-L)}\left[\frac{dW_{1p}(z)/dz}{W_{1p}(z)}\right]_{Z=Z-L} , \quad (2.16)$$

$$\zeta_{s,+}^{-1}(z)=\lim_{L\to 0}\frac{c/\omega}{\mu(z+L)}\left[\frac{dW_{2s}(z)/dz}{W_{2s}(z)}\right]_{Z=Z+L} , \quad (2.17)$$

$$\zeta_{s,-}^{-1}(z)=\lim_{L\to 0}\frac{c/\omega}{\mu(z-L)}\left[\frac{dW_{1s}(z)/dz}{W_{1s}(z)}\right]_{Z=Z-L} . \quad (2.18)$$

The quantities $\zeta_p(z)$ and $\zeta_s(z)$, appearing in the denominators of $G_p(z,z;k_y^2)$ and $G_s(z,z;k_y^2)$, can be identified as dimensionless planar impedances computed at depth z for the corresponding s and p polarizations: $\zeta_{p,+}(z)$ and $\zeta_{s,+}(z)$ are the values of the planar impedances encountered at point z by waves propagating in the crystal growth direction, while $\zeta_{p,-}(z)$ and $\zeta_{s,-}(z)$ are the values encountered at the same point by waves propagating away from the surface. Stated in this way, the polariton structure of multilayers can be constructed in detail for both isolated surface modes and resonant scattering modes, by following the standard prescriptions of a scattering-theoretic approach.

III. PLANAR IMPEDANCE OF A STRATIFIED MEDIUM

All the spectral densities that will be discussed below are based on the description of the planar impedance function at depth z, a scalar quantity which relates to the tangential components of the electric and magnetic fields. The concept of a planar impedance, defined at any plane parallel to the surface, should be recognized as a key ingredient in the calculation of the polariton structure of the complex systems described here. It generalizes the concept of a surface impedance[12,14] introduced in earlier studies of the electromagnetic response of surfaces. For a TM wave, the planar impedance at depth z is defined as the ratio

$$Z_p(z)=\frac{E_y(y,z)}{H_x(y,z)} \tag{3.1}$$

while, for a TE wave, it is given by

$$Z_s(z)=-\frac{E_x(y,z)}{H_y(y,z)} . \tag{3.2}$$

The usefulness of this concept lies in the fact that, for stratified materials, the planar impedance satisfies a simple, first-order Riccati differential equation which provides a general scheme for the calculation of the polariton structure, reflectance and attenuated-total-reflection (ATR) spectra. By using the basic substitution $Z_p(z)=[i/\omega\epsilon_0\epsilon(z)](W_p'/W_p)$ for a TM wave and $Z_s^{-1}(z)=[i/\omega\mu_0\mu(z)](W_s'/W_s)$ for a TE wave, we are led to similar Riccati equations

$$\frac{d\zeta_p}{dz}+\frac{\omega}{c}\epsilon(z)\zeta_p^2=\frac{c}{\omega}\frac{k^2(z)}{\epsilon(z)} \tag{3.3}$$

for the transverse-magnetic polarization, and

$$\frac{d\zeta_s^{-1}}{dz}+\frac{\omega}{c}\mu(z)\zeta_s^{-2}=\frac{c}{\omega}\frac{k^2(z)}{\mu(z)} \tag{3.4}$$

for the transverse-electric polarization. In these equations,

$$\zeta_p(z)=-i(\epsilon_0/\mu_0)^{1/2}Z_p(z) \tag{3.5}$$

and

$$\zeta_s(z)=i(\epsilon_0/\mu_0)^{1/2}Z_s(z)^{1/2} \tag{3.6}$$

are dimensionless planar impedances and coincide with the quantities (2.15)–(2.18) we used in the previous section to express the polariton density of states at depth z. For the most complex systems, the Riccati equations can easily be solved by standard Runge-Kutta procedures[15] if an appropriate initial condition is provided. This initial value of the planar impedance can easily be constructed in the case of stratified structures deposited on an infinitely thick substrate. In order to assess the planar impedances encountered by waves propagating from outside the sample towards the substrate interface, we consider the evanescent solutions $W_p(z)$ and $W_s(z)$ that develop in the homogeneous substrate described by a constant dielectric response ϵ_{sub} and permeability μ_{sub}. We note that the only acceptable solution of the Riccati equations within the substrate are constants, so that, at the interface with the substrate, $z=z_{\text{sub}}$,

$$\zeta_{p,-}(z_{\text{sub}}^-)=\frac{[(ck_y/\omega)^2-\epsilon_{\text{sub}}\mu_{\text{sub}}]^{1/2}}{\epsilon_{\text{sub}}} \tag{3.7}$$

and

$$\zeta_{s,-}^{-1}(z_{\text{sub}}^-)=\frac{[(ck_y/\omega)^2-\epsilon_{\text{sub}}\mu_{\text{sub}}]^{1/2}}{\mu_{\text{sub}}} . \tag{3.8}$$

In these expressions, the determination of the complex square root should be chosen to verify

$$\text{Re}[(ck_y/\omega)^2-\epsilon_{\text{sub}}\mu_{\text{sub}}]^{1/2}>0 .$$

This provides an appropriate initial condition to integrate the Riccati equation from the substrate towards the surface. However, the computation of the density of polariton modes also requires the knowledge of planar impedances encountered by waves propagating in the opposite growth direction. In this case, the initial conditions are provided at $z=0$ by the planar impedances characterizing the external medium:

$$\zeta_{p,+}(0^+)=-\frac{[(ck_y/\omega)^2-\epsilon_v\mu_v]^{1/2}}{\epsilon_v} , \tag{3.9}$$

$$\zeta_{s,+}^{-1}(0^+)=-\frac{[(ck_y/\omega)^2-\epsilon_v\mu_v]^{1/2}}{\mu_v} \tag{3.10}$$

with

$$\text{Re}[(ck_y/\omega)^2-\epsilon_v\mu_v]^{1/2}>0 .$$

ϵ_v and μ_v are the electric and magnetic response functions of the external medium.

The reflection coefficients R_p and R_s at the surface of a stratified material are expressible in terms of the surface impedance[12,14] or equivalently the functions $\zeta_p(z)$ and $\zeta_s(z)$ evaluated at the surface of the sample ($z=0$). If the angle of incidence of the impinging radiation is θ, the surface wave vector is forced to be

$$k_y=(\epsilon_v\mu_v)^{1/2}(\omega/c)\sin\theta$$

and we can calculate the surface impedance at the imposed external radiation frequency. For reflectivity measurements performed in vacuum, we have $\epsilon_v=\mu_v=1$ while for ATR measurements, ϵ_v and μ_v describe the electromagnetic response of the prism material which is generally independent of the incident radiation frequency. In ATR using Otto's configuration, the air gap can be incorporated in the response functions $\epsilon(z)$ and $\mu(z)$ of the stratified medium. For TM and TE polarizations, one finds, respectively,

$$R_p=\left|\frac{\zeta_{p,-}(0^-)+i(\mu_v/\epsilon_v)^{1/2}\cos\theta}{\zeta_{p,-}(0^-)-i(\mu_v/\epsilon_v)^{1/2}\cos\theta}\right|^2 \tag{3.11}$$

and

$$R_s=\left|\frac{\zeta_{s,-}^{-1}(0^-)+i(\epsilon_v/\mu_v)^{1/2}\cos\theta}{\zeta_{s,-}^{-1}(0^-)-i(\epsilon_v/\mu_v)^{1/2}\cos\theta}\right|^2 . \tag{3.12}$$

It can be seen that the reflectance spectrum calculation explicitly reduces to an initial value problem which requires solving the first-order Riccati equations (3.3) or (3.4) where ζ_p or ζ_s^{-1} obviously correspond to the electromagnetic waves propagating from the external medium towards the sample. Note that when $\zeta_{p,-}(0^-)$ [respectively, $\zeta_{s,-}^{-1}(0^-)$] turns out to be real, the reflection becomes total and the incident radiation is unable to propagate into the stratified structure.

IV. PLANAR IMPEDANCE OF MULTILAYERED STRUCTURES

Sharply defined multilayered structures are a special case of stratified media. They consist of a stack of thin

layers with thicknesses $d_1, d_2, \ldots, d_i, \ldots$, deposited on a semi-infinite substrate. Within each layer, the dielectric and magnetic response functions $\epsilon_1, \epsilon_2, \ldots, \epsilon_i, \ldots$, and $\mu_1, \mu_2, \ldots, \mu_i, \ldots$, are considered to be constant, providing an histogramlike shape of the local dielectric function and magnetic permeability (see Fig. 2). Such ideal multilayer systems adequately model the sharp heterostructures grown from semiconducting materials using molecular beam or metal-organic chemical vapor deposition, when the thickness of each layer is much larger than the atomic lattice spacing. In this case, the basic Riccati equations have constant coefficients within the same homogeneous layer, and provide exact connections between the impedance values $\zeta_{p,-}(z)$ and $\zeta_{s,-}^{-1}(z)$ at two successive boundaries:

$$\zeta_{p,-}(z_{i-1}) = g_{p,i}\coth(k_i d_i) - \frac{g_{p,i}^2/\sinh^2(k_i d_i)}{g_{p,i}\coth(k_i d_i)+\zeta_{p,-}(z_i)} \tag{4.1}$$

for TM modes, and

$$\zeta_{s,-}^{-1}(z_{i-1}) = g_{s,i}\coth(k_i d_i) - \frac{g_{s,i}^2/\sinh^2(k_i d_i)}{g_{s,i}\coth(k_i d_i)+\zeta_{s,-}^{-1}(z_i)} \tag{4.2}$$

for TE waves. The wave vector k_i ($\mathrm{Re}k_i > 0$) is the constant value taken by $k(z)$ within the layer [Eq. (2.4)]:

$$k_i = (\omega/c)[(ck_y/\omega)^2 - \epsilon_i\mu_i]^{1/2}$$

and the coefficients $g_{p,i}$ and $g_{s,i}$ are given by

$$g_{p,i} = \frac{c}{\omega}\frac{k_i}{\epsilon_i} \tag{4.3}$$

and

$$g_{s,i} = \frac{c}{\omega}\frac{k_i}{\mu_i} . \tag{4.4}$$

The explicit solution (4.1) or (4.2) of the Riccati equation yields a recurrence relation which can be used to express the surface value of the planar impedance in the form of a continued fraction. If we introduce the notation $a_{p,i} = g_{p,i}\coth(k_i d_i)$ [$a_{s,i} = g_{s,i}\coth(k_i d_i)$] and $b_{p,i} = g_{p,i}/\sinh(k_i d_i)$ [$b_{s,i} = g_{s,i}/\sinh(k_i d_i)$] we obtain the following explicit relations:

$$\zeta_{p,-}(0^-) = a_{p,1} - \cfrac{b_{p,1}^2}{a_{p,1}+a_{p,2} - \cfrac{b_{p,2}^2}{a_{p,2}+a_{p,3} - \cfrac{b_{p,3}^2}{a_{p,3}+a_{p,4} - \cdots}}} \tag{4.5}$$

for the transverse-magnetic polarization, and

$$\zeta_{s,-}^{-1}(0^-) = a_{s,1} - \cfrac{b_{s,1}^2}{a_{s,1}+a_{s,2} - \cfrac{b_{s,2}^2}{a_{s,2}+a_{s,3} - \cfrac{b_{s,3}^2}{a_{s,3}+a_{s,4} - \cdots}}} \tag{4.6}$$

for transverse-electric modes. These continued fractions terminate for a finite number of layers deposited onto an infinitely thick substrate. In that case, as d_{sub} becomes infinite, the coefficient $b_{p,\mathrm{sub}}[b_{s,\mathrm{sub}}]$ vanishes while $a_{p,\mathrm{sub}} = g_{p,\mathrm{sub}}[a_{s,\mathrm{sub}} = g_{s,\mathrm{sub}}]$. The continued-fraction expansion of the surface impedance is particularly useful, as it allows one to investigate in a simple way both finite or infinite systems, using response functions which do or do not incorporate electromagnetic wave absorption.

One particular class of systems giving rise to an infinite continued fraction is the ideal semi-infinite superlattice. In this important case, we are led to a periodic continued fraction which, when convergent, can further be evaluated in closed form.[16] The periodic structure of the continued fraction is implied by the periodicity of the planar impedance. This can be adequately expressed as

$$\zeta_{p,-}(z+L) = \zeta_{p,-}(z) \tag{4.7}$$

and

$$\zeta_{s,-}^{-1}(z+L) = \zeta_{s,-}^{-1}(z) , \tag{4.8}$$

where L is the superlattice period. If one considers a pattern consisting of two layers of thicknesses d_1 and d_2 periodically repeated towards the sample volume, the value of the periodic continued fraction is one of the solutions of a quadratic equation. For the TM mode, this equation is written

$$(a_{p,1}+a_{p,2})\zeta_{p,-}^2 + (g_{p,2}^2 - g_{p,1}^2)\zeta_{p,-} - (a_{p,1}g_{p,2}^2 + a_{p,2}g_{p,1}^2) = 0 \tag{4.9}$$

and, for the TE mode, one has

$$(a_{s,1}+a_{s,2})\zeta_{s,-}^{-2}+(g_{s,2}^2-g_{s,1}^2)\zeta_{s,-}^{-1}-(a_{s,1}g_{s,2}^2+a_{s,2}g_{s,1}^2)=0\ . \tag{4.10}$$

In general, the response functions have an imaginary part, expressing the damping of the electromagnetic radiation. In that case, the coefficients of the quadratic equations are complex and the continued fractions converge towards that solution:

$$\zeta_{p,-}(0^-)=\frac{g_{p,1}^2-g_{p,2}^2}{2(a_{p,1}+a_{p,2})}\pm\left[\left[\frac{g_{p,1}^2-g_{p,2}^2}{2(a_{p,1}+a_{p,2})}\right]^2+\frac{a_{p,1}g_{p,2}^2+a_{p,2}g_{p,1}^2}{a_{p,1}+a_{p,2}}\right]^{1/2} \tag{4.11}$$

or

$$\zeta_{s,-}^{-1}(0^-)=\frac{g_{s,1}^2-g_{s,2}^2}{2(a_{s,1}+a_{s,2})}\pm\left[\left[\frac{g_{s,1}^2-g_{s,2}^2}{2(a_{s,1}+a_{s,2})}\right]^2+\frac{a_{s,1}g_{s,2}^2+a_{s,2}g_{s,1}^2}{a_{s,1}+a_{s,2}}\right]^{1/2} \tag{4.12}$$

closest to their first approximants $a_{p,1}-b_{p,1}^2/(a_{p,1}+a_{p,2})$ [respectively, $a_{s,1}-b_{s,1}^2/(a_{s,1}+a_{s,2})$]. If damping is neglected, the continued fraction will converge when the above roots are real, and will diverge when the roots are complex. The convergence or divergence of the continued fraction is of central importance in the description of the surface-interface polariton structure of semi-infinite superlattices.

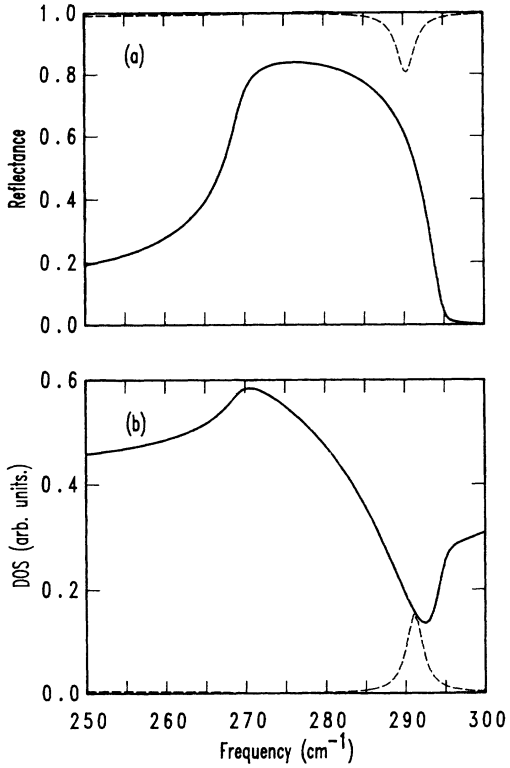

FIG. 2. (a) Calculated infrared TM reflectance (solid curve) and simulated ATR scan (dashed curve) of a semi-infinite GaAs sample. Oscillator parameters of GaAs: $\omega_{TO}=269.2$ cm^{-1}, $\omega_{LO}=293.0$ cm^{-1}, $\epsilon_0=12.9$, $\epsilon_\infty=10.9$, and $\gamma/\omega_{TO}=0.009$. The angle of incidence θ is 60° in each experiment. A 0.5 μm vacuum gap separates a Ge prism ($\epsilon_v=16$) and the GaAs substrate for the ATR simulation. (b) Surface local densities $(\omega/c)\rho_p(z=0;k_y^2)$ of the modes involved in these spectra for $k_y=(\omega/c)\sin\theta$ (solid line) and $k_y=[\omega(\epsilon_v)^{1/2}/c]\sin\theta$ (dashed line).

The explicit expressions obtained in this section show that the planar impedances at any depth in a material, and in particular their limiting values at the surface, can be obtained in closed form even in the most complex layered medium as soon as the bulk dielectric functions of the constituant materials are known from experiment or from model calculations. The reflectivities for both polarizations are obtained by straightforward application of Eqs. (4.5) and (3.11) or (4.6) and (3.12). The ATR spectra are accessible by identification of the air gap with the layer $i=1$ in the calculation of R_p. As mentioned in Sec. II, the calculation of the local density of states at any depth requires the values at the depth coordinate z of the planar impedances encountered by waves propagating in the crystal growth direction [$\zeta_{p,+}(z)$ and $\zeta_{s,+}^{-1}(z)$] and encountered by waves propagating opposite to this direction [$\zeta_{p,-}(z)$ and $\zeta_{s,-}^{-1}(z)$]. When facing the growth's axis, the recurrence scheme developed above to compute the TE and TM planar impedances at the surface can naturally be applied to the determination of these impedances at any depth in the multilayered material. One easily sees that the extension of the procedure to find the planar impedances values as seen from the other direction is provided by changing the sign of the coefficients $a_{s,i}$ and $a_{p,i}$ in the corresponding continued fractions and by considering the external medium as a "substrate."

V. POLARITON DISPERSION RELATIONS IN STRATIFIED MEDIA

The electromagnetic eigenmodes of any semi-infinite sample can be grouped into radiative and nonradiative modes. Radiative modes have a long-range wavelike behavior in the medium outside the sample and are basic for understanding reflectivity measurements. Nonradiative modes have an evanescent amplitude outside the sample. Surface polariton modes are characterized by exponentially-decaying amplitudes, both inside and outside the sample.

Polariton modes of a semi-infinite medium can be described by matching the value of the planar impedance as calculated at the surface from the inside and the outside of the sample. The surface impedances $\zeta_{p,+}(0^+)$ and $\zeta_{s,+}^{-1}(0^+)$ just outside the sample are given by Eq. (3.9) and (3.10). The polariton modes exist when

$$\zeta_{p,+}(0)=\zeta_{p,-}(0) \tag{5.1}$$

for a TM wave and

$$\zeta_{s,+}^{-1}(0)=\zeta_{s,-}^{-1}(0) \tag{5.2}$$

for a TE wave. Each of these conditions involves only the projection k_y of $\mathbf{k}$ along the y axis and thus implicitly gives the polariton dispersion relations $\omega=\omega(k_y)$. Wavelike excitations are usually described by their dispersion relations which are generally calculated in the ideal situation where damping is neglected in the dielectric function. All damping effects being ignored in the local response functions, the existence of true surface excitations requires that the quantities on both sides of the above equations be real. This means that an evanescent mode of wave number k_y can only be found at a frequency lower than $(ck_y)/(\epsilon_v\mu_v)^{1/2}$, that is, in the (k_y,ω) diagram, in the region below the dispersion line describing the light propagation in the medium outside the sample. At frequencies above the light dispersion line, the external medium radiates electromagnetic energy and does not allow to sustain localized modes. The same argument can be used for the propagation of energy towards the sample: when $\zeta_{s,-}$ or $\zeta_{p,-}$ are complex, the sample allows energy transport and this is not compatible with the formation of a strictly localized polariton mode. However neglecting the various damping mechanisms is equivalent to considering excitations of infinite lifetime and provides only qualitative agreement with experiments, particularly in radiative regions. If complex dielectric functions were introduced into the implicit dispersion relations to include phenomenologically finite lifetime effects, solutions for both ω and k_y real would not exist. This means that true normal modes are absent when decay processes are taken into account.[17] Consequently, the energy levels of the excitations spectrum are no longer discrete but have some width which allows the study of excitations by experimental methods (ATR is a well-known example of spectroscopy which is applicable thanks to the various dissipative effects.) However, the broadening of true normal modes is not the only phenomenon which result from decay processes. The existence of virtual radiative modes of finite lifetime even in the absence of corresponding ideal normal modes is necessary to explain reflectance data in *Reststrahlen* regions.[18,19] A common way to assess situations where the knowledge of ideal eigenmodes is not satisfactory is to describe excitations via their local density of states in the system. Using the treatment developed in Sec. II, we propose to relate the local density of polariton modes to dispersions relations in various cases of multilayered materials. This discussion will lead to more complete interpretations of optical experiments.

VI. DENSITY OF POLARITON MODES AND SPECTRAL PROPERTIES OF FINITE MULTILAYERED MATERIALS

In the following sections, we will illustrate phonon-polariton structures of layered ionic or polar materials, such as the multilayered systems considered in Fig. 5 to 14, which consists of ideal alternation of GaAs and AlAs layers with a first layer of GaAs exposed to vacuum. The frequency dependence of the relevant dielectric function $\epsilon(\omega)$ in the infrared region is then dominated by the contributions of the transverse-optical-phonon oscillators. More specifically, for a cubic material with two atoms per unit cell, $\epsilon(\omega)$ is given by the well-known expression

$$\epsilon(\omega)=\epsilon_\infty+\frac{(\epsilon_0-\epsilon_\infty)\omega_{\mathrm{TO}}^2}{\omega_{\mathrm{TO}}^2-\omega^2-i\gamma\omega}\ , \tag{6.1}$$

where ϵ_0 and ϵ_∞ are the static and high-frequency dielectric constants, respectively. In Eq. (6.1), ω_{TO} denotes the transverse-optical-vibration frequency and γ is a phenomenological damping factor.

We note that multilayered materials naturally involve the presence of interfaces, which dramatically differentiate the p and s polarizations. It has long been proved that modes localized at interfaces can only be of TM nature (p modes), due to nonzero component of their electric field perpendicular to the interfaces.[19]

A. TM Polarization

Let us first emphasize that the general equation (5.1) that governs interface TM polariton modes enables us to recover at first glance famous results already obtained in the simplest systems: (i) surface modes arising from the termination of a homogeneous medium

$$\frac{1}{\epsilon_v}+\frac{1}{\epsilon(\omega)}=\frac{\omega^2}{k_y^2c^2} \tag{6.2}$$

and (ii) the ionic-slab polaritons described by Fuchs and Kliewer.[18] Also, more complicated multilayered structures can be investigated by the formalism just outlined, for instance: plasmon-polariton structure of a finite alternation of metal-insulator layers;[20] polariton properties in either finite,[21] semi-infinite,[22–25] or quasiperiodic[26] superlattices.

In order to clarify the usefulness of the concept of polariton density of modes, let us first deal with an ideal, semi-infinite homogeneous sample. The polariton structure of this elementary system is well known. Continua of transverse modes are found outside the *Reststrahlen* region, defined by the interval $[\omega_{\mathrm{TO}},\omega_{\mathrm{LO}}]$, by a surface projection of the bulk dispersion $\omega(|\mathbf{k}|)$ curves. In addition, a single surface branch splits off these continua and, for short wavelengths, approaches the frequency of the macroscopic surface phonon ω_{so}, given by $\epsilon(\omega_{\mathrm{so}})=-1$.

Various spectroscopies can be applied to investigate this excitation spectrum. Reflectance experiments, where light is impinging the surface at an angle θ, with a wavevector component along the surface given by $k_y=(\omega/c)\sin\theta$, probe the region of the (ω,k_y) plane above the line $\omega=k_yc$, which contains radiative modes. This means that at any frequency, reflectivity will sample polariton modes at wave vectors shorter than those of the incident light. The domain below $\omega=k_yc$ is that of nonradiative modes.[19] By introducing a supplementary interface, the prism coupling technique (ATR) (Ref. 27) extends the radiative region and allows observing modes

which closely model nonradiative excitations. In other words, ATR probes somewhat larger wave vectors, transforming nonradiative modes into radiative resonances. The region of still larger k_y is the nonretarded limit explored by Raman and electron-energy-loss-spectroscopy (EELS) experiments.

Calculated reflectance and ATR spectra of a semi-infinite GaAs material are depicted in Fig. 2(a). In the tunable-frequency version of the experiment, the prism coupling technique probes the line $\omega = k_y c / [\sin\theta(\epsilon_v \mu_v)]^{1/2}$ For a thick homogeneous sample, the nonradiative surface mode is excited by a tunneling effect across the air gap between the prism and the sample, leading to a dip in the ATR spectrum [Fig. 2(a)]. The thickness of the gap affects the position of this dip; the prism perturbation of the dispersion relations has been largely detailed elsewhere[28–31] and can only be explained by a response function including all damping effects. The occurrence of the ATR dip can be directly related to the density of polariton modes $\rho(z;k_y^2)$ computed at the surface with $k_y = (\omega/c)\sin\theta(\epsilon_v \mu_v)^{1/2}$. Indeed, $\rho(z=0;k_y^2)$ assumes important values when ω is close to $\omega_{SO} = 291$ cm^{-1} [Fig. 2(b)]. The local density ρ computed from Eq. (2.11) at the frequency ω_{SO} is represented as a function of depth z in Fig. 3(a) (dashed line). The local density of this *surface* mode takes significant values in the vicinity of $z = 0$ only.

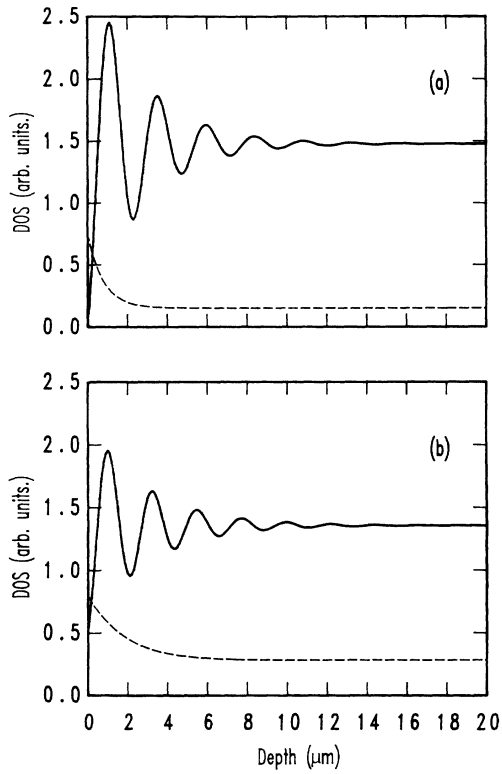

FIG. 3. Density function $(\omega/c)\rho_p(z;k_y^2)$ as function of the depth z in a thick GaAs sample for (a) $k_y = [\omega(\epsilon_v)^{1/2}/c]\sin\theta$ with $\epsilon_v = 16$ relevant for an ATR experiment and (b) $k_y = (\omega/c)\sin\theta$ (ir-reflectance measurements). Two frequencies are considered: $\omega_s = 291$ cm^{-1} (dashed lines) and $\omega = 265$ cm^{-1} (solid lines). The dashed curves have been magnified five times, for clarity.

Polariton local densities of states of *volume* transverse modes have typical behavior depicted in Fig. 3(a) (solid curve). Their oscillatory character close to $z = 0$ is due to interference generated by the surface that reflects internal polariton modes. As the coordinate z increases within the sample, this effect decreases and the density of states converges towards a constant value typical of that of the bulk crystal. This phenomenon is a general consequence of the presence of a surface, which locally modifies the density of modes ρ as compared to that of an unbounded medium. For volume transverse modes, the local density of polariton modes as a function of depth enables one to clarify the differences between radiative and nonradiative eigenmodes. Indeed, local densities of nonradiative modes take very small values at the surface [Fig. 3(a)] which explains why they have no signature in ATR spectra: the incident light cannot find an adequate relay to be transmitted deeper into the medium. On the contrary, local density of a radiative mode at the same frequency exhibits large values at the surface: impinging light can encounter possible supports that will propagate a certain amount of incident energy into the crystal, which causes a decrease of reflectance.

Similar considerations also apply to reflectance data in the *Reststrahlen* region where no true normal modes, other than the surface ones, are expected. At a given frequency in this domain, nonradiative modes have nearly zero local densities at the surface. At the same frequency, radiative-polariton densities of modes exhibit important values just below the surface and take very small values deeper in the crystal, allowing some absorption of energy which accounts for less than total reflectance.

We now turn to a self-supported GaAs film, a geometry first studied by Fuchs and Kliewer.[18,19] In this system, the two GaAs-vacuum interfaces yield two branches of, respectively, odd and even symmetries.[19] In this respect, the two peaks in the density of states computed at the location of one of these interfaces [Fig. 4(a)] are associated with the corresponding slab eigenmodes. It is interesting to notice the strong difference between the amplitudes of these two peaks. In addition, the behavior of the related densities of states as a function of z [Fig. 4(b)] drastically differ as well: the symmetric mode (solid curve) is characterized by a strong localization at the surfaces, whereas the antisymmetric mode assumes nearly constant $\rho(z)$ values inside the slab.

In the more general situation of a thin film (dielectric function ϵ_1) deposited onto a thick substrate (dielectric function ϵ_2), three branches of polariton modes are expected. One is akin to the surface mode already described, and the two other modes result from the interface between two dispersive media. When k_y approaches infinity indeed, the frequencies of the latter branches converge towards those characteristic of interface modes:

$$\epsilon_1(\omega) = -\epsilon_2(\omega) \ . \tag{6.3}$$

In the case of the two infrared active materials, Eq. (6.3) has solutions in the two *Reststrahlen* regions. Bending of the three branches $\omega(k_y)$ becomes significant when the wavelength is of the order of the layer thickness. At still larger wavelengths, retardation effects also induce disper-

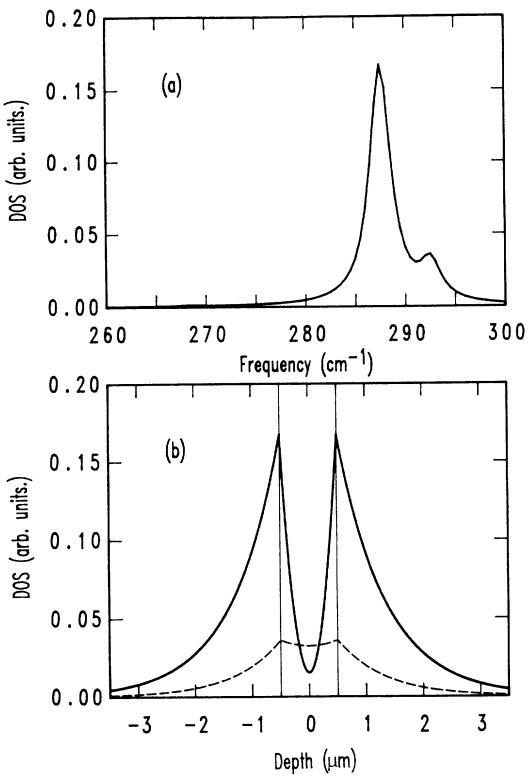

FIG. 4. (a) Surface local density $(\omega/c)\rho_p(z=0.5\ \mu m;k_y^2)$ of the modes probed in an ATR scan of a 1-μm-thick self-supported GaAs slab. (b) Spatial repartition of modes as a function of depth of the symmetric (solid line) and antisymmetric (dashed line) modes excited in the ATR frequency scan on the same GaAs slab.

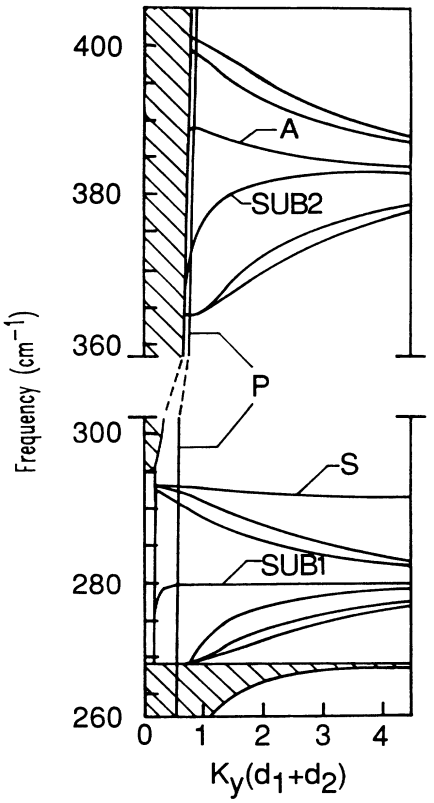

FIG. 5. Polariton dispersion relation of a three-period GaAs-AlAs superlattice deposited on a semi-infinite GaAs substrate. Layer thicknesses: $d_1=0.3333\ \mu$m (GaAs) and $d_2=0.6667\ \mu$m (AlAs). The AlAs *Reststrahlen* extends from 364 cm^{-1} (ω_{TO}) to 403 cm^{-1} (ω_{LO}). The ATR spectrum of Fig. 6 samples the line *P*.

sion in the surface and interface modes, due to the admixture of photon states.

In multilayered structures, increasing the number of interfaces causes supplementary branches to appear (two branches per additional interface). As an illustrative example, Fig. 5 shows the polariton dispersion curves for a threefold alternation of two layers (GaAs and AlAs, $d_1/d_2=0.5$) deposited onto a thick GaAs substrate. Thirteen polariton branches arise here.

The simulated ATR spectrum of this heterostructure depicted in Fig. 6(a) corresponds to a frequency scan along the *P* line $\omega=k_y c/[(\epsilon_v)^{1/2}\sin\theta]$ drawn in the dispersion relations (Fig. 5). Modes with extremely small local densities at the surface do not contribute to the ATR spectrum, whereas dips due to a long-range mode in the substrate (SUB1 in Fig. 5) or an isolated branch (*A* in Fig. 5) are clearly detectable at 280 and 389 cm^{-1}, respectively. Clustered branches, including the surface mode (*S* in Fig. 5) are not separated for this value of the space layer: they appear together in a broad dip.

The too-short decay distance in AlAs of the evanescent modes associated with the substrate interface prevents the observation of the related branch (SUB2 in Fig. 5). In the ATR scan, the detection of interface modes related to the substrate can be understood by considering the polariton local density of states as a function of depth [(Fig. 6(b)]: whereas the SUB2 mode is characterized by vanishingly small amplitudes near the surface (solid curve), the SUB1 mode possesses a surface amplitude which, although small is sufficient to allow for a coupling with the prism and thus, for the presence of a dip in the ATR spectrum. Notice that such calculation enables to identify each branch of Fig. 5 in terms of the location where their localizations dominate. Such study of the localization and finite-size effects of collective modes in finite layered structures has been performed in the electrostatic limit by Johnson, Weiler, and Camley.[21] These authors identify localized plasmon modes by investigating the associated electrostatic potentials. However, in order to interpret optical properties, the electrostatic approximation is not sufficient. Using the density of polariton modes, i.e., the density of those excitations involved in optical experiments, the approach presented here extends the study of localized modes to the fully-retarded spectrum.

B. TE polarization

s-polarized spectral properties in relation with their dispersion relations can also be investigated using polariton local densities of states. As explained above, isotropic materials do not sustain any TE-polarized interface modes (no ATR signatures), so that it is only worth con-

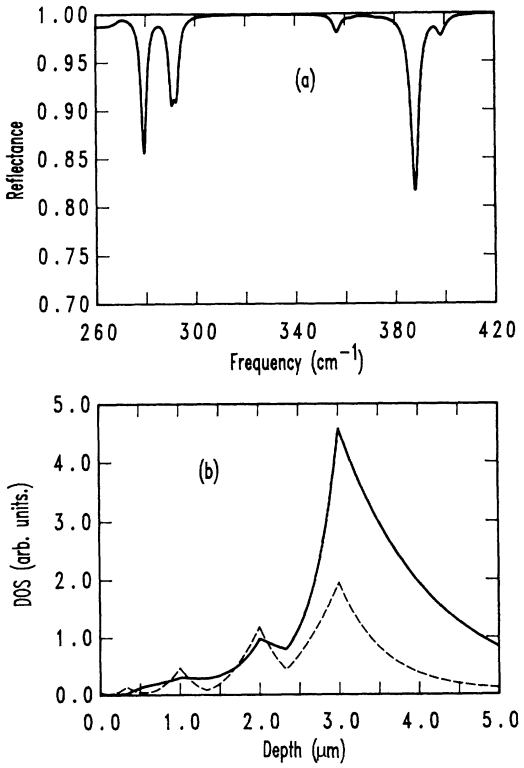

FIG. 6. (a) ATR experiment ($\epsilon_v = 16$, $\theta = 60°$, space layer is 1 μm) on the multilayered material whose polariton structure was considered in Fig. 5. (See text for details.) (b) The polariton local densities of modes of the SUB1 (dashed line) and SUB2 (solid line) modes involved in the ATR experiment show that both modes are associated with the substrate interface (depth 3.0 μm).

sidering reflectance spectra. With identical experimental parameters (incidence angle, frequency), higher reflectivity characterizes *s*-polarized light as compared to *p*-polarized light. This classical result can also be assessed in terms of volume and virtual modes: TE polariton local densities of states are much smaller to TM densities calculated in the same conditions.

VII. POLARITON DENSITY OF MODES AND SPECTRAL PROPERTIES OF SUPERLATTICES

The ability to build atomically-accurate artificial structures using advanced crystal growth techniques has opened a wide field of research interests. Among those, the ideal semi-infinite superlattice consisting of the periodic alternation of different constituent materials is already recognized as an important achievement which promises to reveal many types of new collective excitations.[2,8,9] The general methods developed in this paper will now be used to visualize the generation of such excitations in superlattices in the domain of retarded phonon polaritons. The limiting case of nonretarded collective excitations in superlattices has recently been considered in connection with results of Raman scattering[3–5] and electron-energy loss[6,7] measurements on semiconducting GaAs-GaAlAs superlattices.

A. TM polarization

Retarded dispersion relations of plasmon-polaritons in superlattices have been computed by Szenics *et al.*[23] and recently detailed by Haupt and Wendler.[24] The case of phonon polaritons[32] follows the same qualitative scheme: when the number of interfaces is increased in such a way as to approach the geometry of a semi-infinite superlattice of period L, many new interface modes group into continuum regions, leaving a few isolated branches. As an example, Fig. 7 shows the polariton dispersion relations computed for an idealized GaAs/AlAs superlattice. The various polariton modes can easily be identified by considering the short-wavelength limit ($k_y \gg 2\pi/L$) of their frequencies. The continuum regions converge towards the isolated GaAs/AlAs interface frequencies [Eq. (6.3)]. The narrowing of the continuum regions and their convergence towards the isolated interface frequencies indicate the dominance of pure interface modes in these short-wavelength excitations and the progressive disappearance of the overlap of the interface mode when the wavelength is reduced well below the layer thicknesses. On the other hand, for wavelengths large enough to approach the light line, retardation effects start to show up. As indicated in Fig. 7, the layer thicknesses determine the amount of overlap between the interface modes and control the width of the continua. An interface mode extending preferentially in a thin layer has a frequency much more sensitive to any variation of its wavelength, which is intimately connected with the penetration depth away from the interface. For $d_1/d_2 = 0.5$, the GaAs layer is thinner than the AlAs layer; the continua in the AlAs *Reststrahlen* region (364–403 cm^{-1}) are relatively narrow and well separated. By contrast, in the GaAs *Reststrahlen* region (269–293 cm^{-1}), the overlap between interacting interface modes is much more effective and the continuum bands tends to be wider. This results also in a band scheme radically different from that of the former *Reststrahlen*. Similar observations can be done for the opposite situation $d_1/d_2 = 2$.

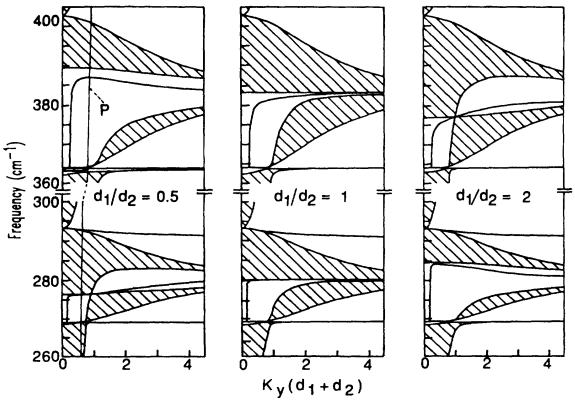

FIG. 7. Polariton diagram of three semi-infinite GaAs-AlAs superlattice with various layer thicknesses ($d_1 + d_2 = 1$ μm). Blochlike continua of interface modes are described by the shaded areas, the localized interface modes are indicated by solid lines. The *P* line is explored by the ATR experiment shown in Fig. 12(b), where a Ge prism is used.

Before analyzing the dispersion relations of semi-infinite superlattices in terms of polariton local densities of states, it is worth examining what happens in unbounded, truly periodic superlattices. In the region of volume transverse modes (i.e., any mode in the shaded areas of Fig. 7 outside the *Reststrahlen*), the polariton local density of modes as a function of depth reflects the medium inhomogeneity. Depending on wavelength, one of the superlattice materials can be better suited to sustain the mode than the other constituent. This corresponds to some sort of confinement of polariton modes in the former layers, as examplified in Fig. 8(a), where maxima of the polariton density of modes are found inside the GaAs layers. By contrast, volume modes in a *Reststrahlen* domain are more akin to interface modes, as the related polariton densities peak at the interfaces (Fig. 9). Because penetration depths are large in regard to the layer thicknesses, densities of these interface modes keep non-negligible values across the layers. This phenomenon occurs in the nonradiative regions as well as in the radiative region, where a similar result is obtained (Fig. 9), as a consequence of combinations of virtual modes when dampings in the ϵ's are included. In both regions, the main fact is that the periodicity of interfaces establish important values of the polariton density of states, everywhere in the superlattice, at frequencies and wavelengths where excitation densities of the same magnitude would be impossible in the separate constituents.

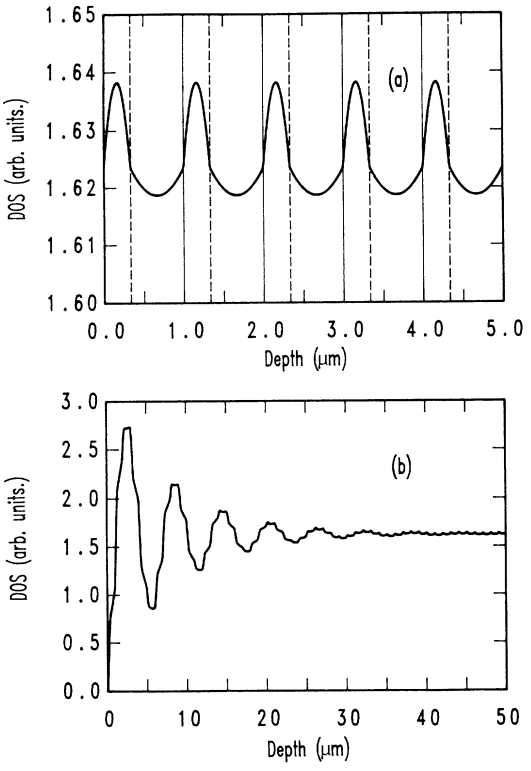

FIG. 8. (a) Plot of $(\omega/c)\rho_p(z;k_y^2)$ with $k_y=(4\omega/c)\sin\theta(\theta=60°)$ for a nonradiative volume mode of frequency 265 cm^{-1} in an unbounded superlattice whose period is made of 0.3333-μm-thick GaAs layer followed by 0.6667-μm-thick AlAs layer. Solid vertical lines visualize the periods, i.e., the AlAs-GaAs interfaces whereas dashed lines indicate the GaAs-AlAs interfaces. (b) Local density of polariton modes as a function of depth of a nonradiative volume mode ($\omega=265$ cm^{-1}) for the semi-infinite superlattice structure with the same period characteristics. The pattern of Fig. 8(a) is strongly perturbed by the presence of the surface located at depth 0.0 μm.

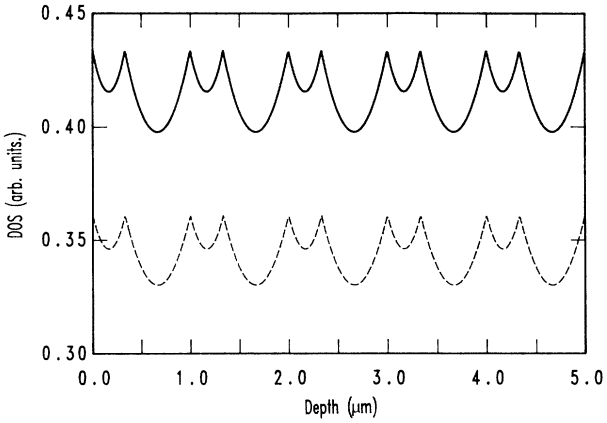

FIG. 9. For the same unbounded superlattice as in Fig. 8(a) $(\omega/c)\rho_p(z;k_y^2)$ as a function of z proves that the Bloch combination of interface modes arises in the radiative region (dashed line, $k_y=\omega\sin\theta/c$) and in the nonradiative case (solid line, $k_y=\omega(\epsilon_v)^{1/2}\sin\theta/c$]. Here $\omega=280$ cm^{-1} and the prism is made of Ge ($\epsilon_v=16$).

Considering now a terminated superlattice, the first obvious fact that can be inferred from the homogeneous system described above is the appearance of excitations mainly localized in the vicinity of the surface, which were absent in infinite superlattices. Closer analysis of the polariton local density of modes shows that these excitations are preferentially distributed at the GaAs-AlAs interfaces (Fig. 10). Notice that the only branch associated with the vacuum-GaAs interface is the upper branch in the GaAs *Reststrahlen* (Fig. 7), which is easily probed by electrons in an EELS experiment.[7] The next consequence arising from the surface-induced perturbation can be similarly inferred from the problem of a semi-infinite homogeneous crystal. Polariton local densities of modes in the continua undergo modulation in the vicinity of the free surface and recover the behavior of the unbounded medium deeper in the sample. This principle applies to confined modes [Fig. 8(b)] and to interface modes as well (Fig. 11).

Using information provided by the description of local densities of modes, we have all the required elements at hand to interpret TM spectral properties of superlattices. As shown in Fig. 12(b) (solid curve), ATR experiments can reveal continua of interface modes, although the attenuation of the signal is less than for the dips attributed to isolated modes found in nonradiative regions. The surface branch is excited after radiation has tunneled across the gap, yielding the dip at 292 cm^{-1} in the spectrum. The pronounced dip at $\omega=387$ cm^{-1} is the signature of the isolated branch in the AlAs *Reststrahlen* of Fig. 7, though the density function of this mode (Fig. 10) reaches a maximum below the first layer and not at the surface.

The interpretation of p reflectance [dashed curve in

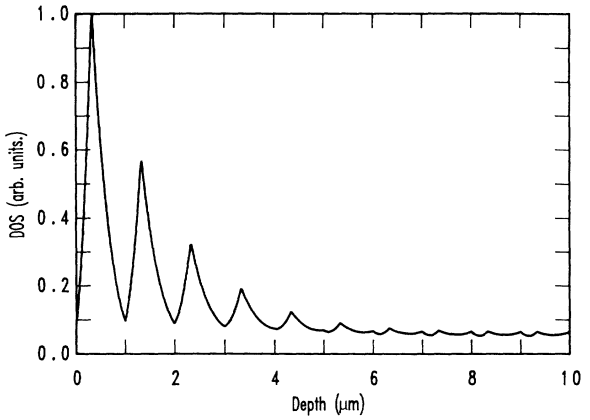

FIG. 10. For the system of Fig. 7, where $d_1=0.3333$ μm and $d_2=0.6667$ μm, the decay of $(\omega/c)\rho_p(z;k_y^2)$ for the mode belonging to the isolated branch at $\omega=387$ cm^{-1} as a function of depth shows the mode localization distributed over the interfaces, with the maximum density of the mode at the first GaAs-AlAs interface [$k_y=\omega(\epsilon_v)^{1/2}\sin\theta/c$ and $\epsilon_v=16$].

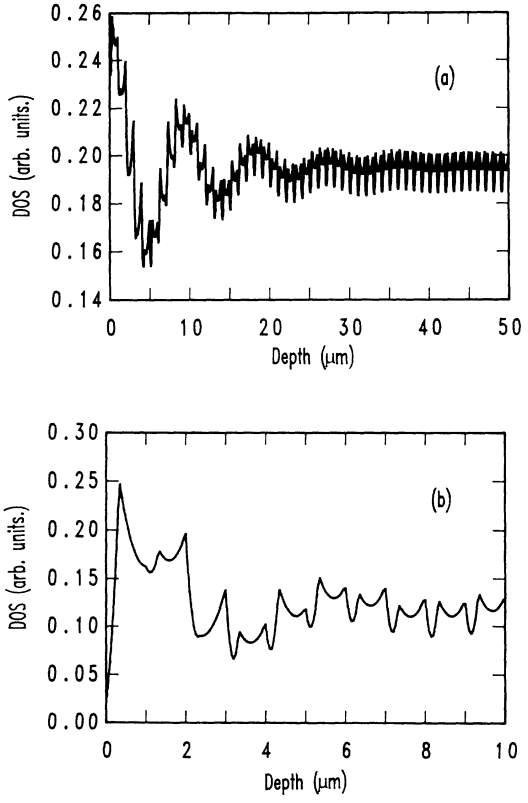

FIG. 11. Evolution of $(\omega/c)\rho_p(z;k_y^2)$ as a function of z for (a) radiative ($k_y=\omega\sin\theta/c$) and (b) nonradiative [$k_y=\omega(\epsilon_v)^{1/2}\sin\theta/c$ and $\epsilon_v=16$] interface modes of frequency 395 cm^{-1} (AlAs *Reststrahlen*) for the same superlattice as in the previous figure. Both modes have a nonzero local density on the surface and are therefore detected in reflectance and ATR experiments.

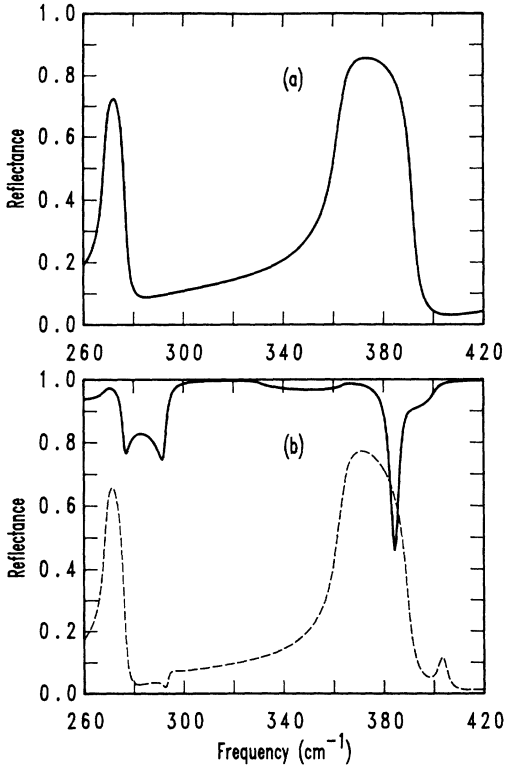

FIG. 12. Simulated spectra of the GaAs-AlAs superlattice with $d_1=0.3333$ μm and $d_2=0.6667$ μm at $\theta=60°$. (a) TE reflectance; (B) TM reflectance (dashed line) and ATR scan (solid line) with a Ge prism showing clear evidence of the absorption by the continua of interface modes. In the simulated ATR spectrum, Bloch continua cause smooth attenuation whereas the isolated modes are enhanced.

Fig. 12(b)] of a superlattice follows the argumentation developed for the homogeneous crystal in the preceding section. Incident light must find excitation relays at the surface, and deeper in the sample, to propagate into the medium. In the radiative region, these supports are provided by confined transverse modes and also by resonant interface modes [Fig. 11(a)], so that, in the *Reststrahlen* frequency domains, transmission of light is allowed at frequencies which should be reflected by the individual constituent materials. Before turning our attention to TE polarization, we note that both p-reflectance experiments and ATR scans are convenient to detect continua of interface modes.[32]

B. TE polarization

The s-reflectance spectrum of the GaAs-AlAs superlattice already considered is depicted in Fig. 12(a). The dispersion relations, deduced from Eq. (5.2), of a superlattice in TE polarization are shown in Fig. 13. From this diagram, it transpires that s reflectance also decreases in both *Reststrahlen* frequency domains. For s-polarized excitations in a superlattice composed of isotropic semiconductors, transmission of frequencies in the *Reststrahlen* of a given component material cannot be due to interface modes but results from volume polaritons confined in the

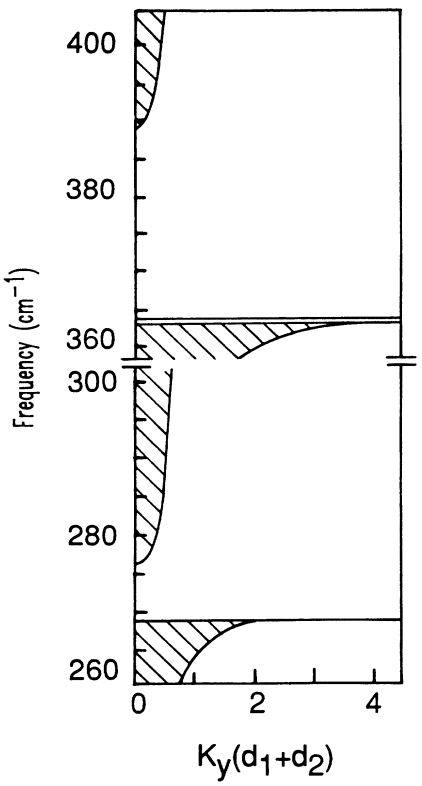

FIG. 13. Dispersion relations of the superlattice structure of Fig. 7 (with $d_1/d_2=0.5$) in TE polarization. This diagram is identical to the one obtained for the ordinary wave of an effective anisotropic medium (see Sec. VII).

made from the other constituent. At long wavelengths relevant here, confined excitations can propagate throughout the superlattice, by tunneling across the opaque layers (dashed curve, Fig. 14), until a given frequency limit is reached where internal reflections make any propagation impossible (solid line, Fig. 14). Outside the *Reststrahlen* regions, the local densities of states of *s*-polarized excitations in superlattices reflect the inhomogeneity of the sample, in the same way as the densities of *p*-polarized excitations do (similar to those shown in Fig. 8).

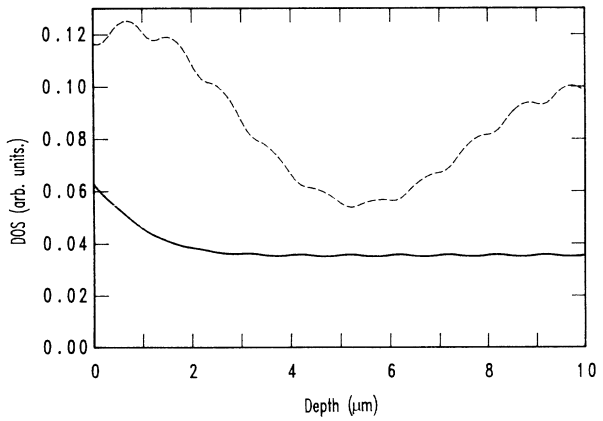

FIG. 14. Evolution of $(\omega/c)\rho_s(z;k_y^2)$ as a function of depth for the semi-infinite superlattice whose dispersion relations are displayed in the previous figure, for two frequencies situated in the GaAs *Reststrahlen:* $\omega=280$ cm^{-1} (dashed line); $\omega=272$ cm^{-1} (solid line). Both modes are radiative ($k_y=\omega\sin\theta/c$, $\theta=60°$).

C. Reflectivity of superlattices and artificial anisotropy

For both TM and TE polarizations, the reflectivity of a semi-infinite superlattice replicating two different layers shows two nearly total reflection regions, located just above the transverse-optical frequencies of the constituent materials [Figs. 12(a) and 12(b)]. These *Reststrahlen* regions do not extend to the corresponding longitudinal-optical frequency, but are cut off at a frequency which depends on the relative thicknesses of the layers (see dispersion relations of Fig. 7).

In the long-wavelength limit, that is for an incident radiation of wavelength much larger than the superlattice period, these results can be given a simple interpretation, in agreement with early descriptions of the optical behavior of nonterminated interleaved stacks of transparent plates.[33] The semi-infinite correspondence can best be obtained by reconsidering the above Riccati's equations [Eqs. (3.3) and (3.4)].

At the long-wavelength limit ($\omega/c\to 0$), the Riccati equations reduce to $d\zeta(z)/dz=0$, so that their solutions become constant. This means that, in the case of a thin heterogeneous film deposited onto a thick substrate, the reflectance spectrum will be that characterizing the substrate, whatever the structure of the deposited film may be, provided its thickness is much smaller than the incident radiation wavelength.

For an ideal semi-infinite superlattice with a period L much smaller than the incident wavelength, $\zeta(z)$ also tends to a constant, but determining its value requires some more algebra. The Riccati equations can be written in the form of an integral equation. For the TM mode, we have

$$\zeta_{p,-}(z)=\zeta_{p,-}(0)+\frac{\epsilon_v\mu_v\omega}{c}\sin^2\theta\int_0^z\frac{1}{\epsilon(z)}dz - \frac{\omega}{c}\int_0^z\mu(z)dz-\frac{\omega}{c}\int_0^z\epsilon(z)\zeta_{p,-}^2(z)dz\ , \tag{7.1}$$

whereas, for a TE wave, we obtain

$$\zeta_{s,-}^{-1}(z)=\zeta_{s,-}^{-1}(0)+\frac{\epsilon_v\mu_v\omega}{c}\sin^2\theta\int_0^z\frac{1}{\mu(z)}dz - \frac{\omega}{c}\int_0^z\epsilon(z)dz-\frac{\omega}{c}\int_0^z\mu(z)\zeta_{s,-}^{-2}(z)dz\ . \tag{7.2}$$

For vanishing values of $\frac{\omega}{c}$, these equations can be solved efficiently by a perturbative iteration technique. The first approximation in this case is $\zeta_{p,-}(z)\simeq\zeta_{p,-}(0)$ [respectively $\zeta_{s,-}^{-1}(z)\simeq\zeta_{s,-}^{-1}(0)$], and the next approximation is obtained by inserting this value in the right-hand side of the integral equations. Next, expressing that these solutions must be periodic in the case of a general periodic stratified structure, namely, $\zeta_{p,-}(L)=\zeta_{p,-}(0)$, provides us with an equation that allows computing the first-

approximation solution. For a TM wave, one obtains

$$\zeta_{p,-}(0)=\frac{(\langle\epsilon\rangle\langle\epsilon^{-1}\rangle\epsilon_v\mu_v\sin^2\theta-\langle\epsilon\rangle\langle\mu\rangle)^{1/2}}{\langle\epsilon\rangle} \tag{7.3}$$

and, for a TE wave,

$$\zeta_{s,-}^{-1}(0)=\frac{(\langle\mu\rangle\langle\mu^{-1}\rangle\epsilon_v\mu_v\sin^2\theta-\langle\epsilon\rangle\langle\mu\rangle)^{1/2}}{\langle\mu\rangle}\ . \tag{7.4}$$

In Eqs. (7.3)–(7.4), expressions $\langle\cdots\rangle$ denote the average over a superlattice period.

By making the substitution $\langle\epsilon\rangle=\epsilon_\parallel$ and $\langle\epsilon^{-1}\rangle=\epsilon_\perp^{-1}$, and similar substitutions for the magnetic permeabilities, the expressions (7.3) and (7.4) reproduce the surface impedance or admittance of a uniaxial material presenting its c axis perpendicular to the free surface.[34–36] In these notations, the effective dielectric and magnetic tensors have the form

$$\begin{bmatrix}\epsilon_\parallel & 0 & 0\\ 0 & \epsilon_\parallel & 0\\ 0 & 0 & \epsilon_\perp\end{bmatrix}\quad\text{and}\quad\begin{bmatrix}\mu_\parallel & 0 & 0\\ 0 & \mu_\parallel & 0\\ 0 & 0 & \mu_\perp\end{bmatrix}, \tag{7.5}$$

where $\epsilon_\parallel$ and $\mu_\parallel$ are the response function values to be considered for field components parallel to the surface while $\epsilon_\perp$ and $\mu_\perp$ are the corresponding quantities for field components perpendicular to the surface. For a nonmagnetic superlattice made of two layers of thicknesses d_1 and d_2 and dielectric constants ϵ_1 and ϵ_2 ($\mu_1=\mu_2=1$), these reduce to the simple arithmetic means

$$\epsilon_\parallel=\langle\epsilon\rangle=\left[\frac{d_1}{d_1+d_2}\right]\epsilon_1+\left[\frac{d_2}{d_1+d_2}\right]\epsilon_2 \tag{7.6}$$

and

$$\frac{1}{\epsilon_\perp}=\langle\epsilon^{-1}\rangle=\left[\frac{d_1}{d_1+d_2}\right]\frac{1}{\epsilon_1}+\left[\frac{d_2}{d_1+d_2}\right]\frac{1}{\epsilon_2}\ . \tag{7.7}$$

At long wavelength, the response of such a superlattice to an electric field parallel to its surface and interfaces (dielectric response $\epsilon_\parallel$) is then analogous to that observed in an arrangement of two capacitors with plate areas proportional to d_1 and d_2, filled with a material of dielectric constant ϵ_1 and ϵ_2, respectively, and arranged in a parallel-type setup. For a field normal to the layers (dielectric response $\epsilon_\perp$) it is analogous to a series arrangement of capacitors of thicknesses d_1 and d_2.

One finds an anisotropy induced by the geometric structure of the superlattice even if, as is usually the case, the multilayer is made from materials that have isotropic responses. For the TE polarization, the approximation of the effective uniaxial medium should remain valid until somewhat large k_y vector, as the true dispersion relations of the superlattice obtained from Eq. (5.2) coincide with the dispersion relation of the ordinary wave in a uniaxial crystal whose $\epsilon_\parallel$ obeys Eq. (7.6). This is compatible with the fact that TE waves do not generate any extraordinary wave in an uniaxial crystal.[37] By contrast, the effective-medium approximation should be limited to the radiative region only for the TM polarization. This can be understood by considering that the dispersion relation of the extraordinary wave of a uniaxial crystal, whose $\epsilon_\perp$ verifies (7.7), should depend on the direction of propagation of the collective excitations involved.[37] Clearly, this cannot hold when these excitations are of interfacial nature. The detailed study of the role of interfaces developed in this paper shows that the interpretation in terms of an effective medium will encounter difficulties when facing experiments such as attenuated total reflection.

ACKNOWLEDGMENTS

This work was funded by the Belgian program on Interuniversity Attraction Poles initiated by the Belgian State Prime Minister's Office (Science Policy Programming). The authors acknowledge the use of the Namur Scientific Computing Facility (Namur-SCF), a common project between the Fonds National Belge de la Recherche Scientifique (FNRS), IBM-Belgium, and the Facultés Universitaires N.-D. de la Paix.

[1] L. Esaki, in *Recent Topics in Semiconductor Physics,* edited by H. Kamimura and Y. Toyozawa (World Scientific, Singapore, 1983), pp. 1–71.
[2] G. Abstreiter, R. Merlin, and A. Pinczuk, IEEE J. Quantum Electron. **QE-22**, 1771 (1986).
[3] A. K. Sood, J. Menéndez, M. Cardona, and K. Ploog, Phys. Rev. Lett. **54**, 2115 (1985).
[4] J. K. Jain and Ph. B. Allen, Phys. Rev. Lett. **54**, 2437 (1985).
[5] A. Pinczuk, M. G. Lamont, and A. C. Gossard, Phys. Rev. Lett. **56**, 2092 (1986).
[6] Ph. Lambin, J. P. Vigneron, and A. A. Lucas, Phys. Rev. B **32**, 8203 (1985).
[7] Ph. Lambin, J. P. Vigneron, A. A. Lucas, P. A. Thiry, M. Liehr, J. J. Pireaux, R. Caudano, and T. J. Kuech, Phys. Rev. Lett. **56**, 1842 (1986).
[8] G. F. Giuliani and J. J. Quinn, Phys. Rev. Lett. **51**, 919 (1983).
[9] A. C. Tselis and J. J. Quinn, Phys. Rev. B **29**, 3318 (1984).
[10] M. Born and E. Wolf, *Principles of Optics* (Pergamon, London, 1958), p. 50.
[11] F. Abelès, Ann. Phys. (Paris), 596 (1950); 706 (1950).
[12] L. M. Brekhovskikh, *Waves in Layered Media* (Academic, New York, 1980).
[13] Ph. Lambin, J. P. Vigneron, A. A. Lucas, and A. Dereux, Phys. Scr. **35**, 343 (1987).
[14] L. Landau and E. Lifschitz, *Electrodynamics of Continuous Media* (Pergamon, Oxford, 1960), p. 279.
[15] G. E. Forsythe, M. A. Malcolm, and C. B. Moler, *Computer Methods for Mathematical Computations* (Prentice-Hall, Englewood Cliffs, 1977).
[16] H. S. Wall, *Analytic Theory of Continued Fractions* (Chelsea, New York, 1973), p. 35.
[17] G. Borstel and H. J. Falge, in *Electromagnetic Surface Modes,* edited by A. D. Boardman (Wiley, New York, 1982), p. 219, and references therein.
[18] R. Fuchs and K. L. Kliewer, Phys. Rev. **140**, A2076 (1965).
[19] R. Fuchs and K. L. Kliewer, Adv. Chem. Phys. **27**, 355 (1974).

[20]E. N. Economou, Phys. Rev. **182**, 439 (1969).
[21]B. L. Johnson, J. T. Weiler, and R. E. Camley, Phys. Rev. B **32**, 6544 (1985).
[22]R. E. Camley and D. L. Mills, Phys. Rev. B **29**, 1695 (1984).
[23]R. Szenics, R. F. Wallis, G. Giuliani, and J. J. Quinn, Surf. Sci. **166**, 45 (1986).
[24]R. Haupt and L. Wendler, Phys. Status Solidi B **142**, 125 (1987).
[25]R. Haupt and L. Wendler, Phys. Status Solidi B **142**, 423 (1987).
[26]S. Das Sarma, A. Kobayashi, and R. E. Prange, Phys. Rev. B **34**, 5309 (1986).
[27]A. Otto, Z. Phys. **216**, 398 (1968).
[28]R. W. Gammon and E. D. Palik, J. Opt. Soc. Amr. **64**, 350 (1974).
[29]E. T. Arakawa, M. W. Williams, R. N. Hamm, and R. H. Ritchie, Phys. Rev. Lett. **31**, 1127 (1973).
[30]R. W. Alexander, G. S. Kovener, and R. J. Bell, Phys. Rev. Lett. **32**, 154 (1974).
[31]A. D. Boardman, in *Electromagnetic Surface Modes,* edited by A. D. Boardman (Wiley, New York, 1982), p. 1.
[32]A. Dereux, J. P. Vigneron, Ph. Lambin, and A. A. Lucas, Phys. Scr. **35**, 338 (1987).
[33]S. M. Rytov, Zh. Eksp. Teor. Fiz. **29**, 605 (1955) [Sov. Phys.—JETP **2**, 466 (1956)].
[34]P. Apell, O. Hunderi, and R. Monreal, Phys. Scr. **34**, 903 (1986).
[35]V. M. Agranovitch and V. E. Kravtsov, Solid State Commun. **55**, 85 (1985).
[36]K. A. Maslin, T. J. Parker, N. Raj, D. R. Tilley, P. J. Dobson, D. Hilton, and C. T. B. Foxon, Solid State Commun. **60**, 461 (1985).
[37]H. Poulet and J. P. Mathieu, *Vibrations Spectra and Symmetry of Crystals* (Gordon and Breach, New York, 1976), Chap. 6.